Transfer-free growth of graphene on SiO₂ insulator substrate from sputtered carbon and nickel films

Genhua Pan [a],*, Bing Li [a], Mark Heath [a,b], David Horsell [b], M. Lesley Wears [b], Laith Al Taan [a], Shakil Awan [a,c]

[a] *Wolfson Nanomaterials & Devices Laboratory, School of Computing & Mathematics, University of Plymouth, Devon PL4 8AA, UK*
[b] *College of Engineering, Mathematics and Physical Sciences, University of Exeter, Exeter EX4 4QF, UK*
[c] *Cambridge Graphene Centre, University of Cambridge, Cambridge CB3 0FA, UK*

ARTICLE INFO

ABSTRACT

Here we demonstrate the growth of transfer-free graphene on SiO₂ insulator substrates from sputtered carbon and metal layers with rapid thermal processing in the same evacuation. It was found that graphene always grows atop the stack and in close contact with the Ni. Raman spectra typical of high quality exfoliated monolayer graphene were obtained for samples under optimised conditions with monolayer surface coverage of up to 40% and overall graphene surface coverage of over 90%. Transfer-free graphene is produced on SiO₂ substrates with the removal of Ni in acid when Ni thickness is below 100 nm, which effectively eliminates the need to transfer graphene from metal to insulator substrates and paves the way to mass production of graphene directly on insulator substrates. The characteristics of Raman spectrum depend on the size of Ni grains, which in turn depend on the thickness of Ni, layer deposition sequence of the stack and RTP temperature. The mechanism of the transfer-free growth process was studied by AFM in combination with Raman. A model is proposed to depict the graphene growth process. Results also suggest a monolayer self-limiting growth for graphene on individual Ni grains.

1. Introduction

Graphene has attracted huge interest because of its wide range of potential applications ranging from electronics and photonics to solar cells and energy storage [1–6]. To take many of these applications to an industrial level requires large scale growth of high quality graphene directly on device compatible substrates without the need for transfer as the extra transfer step unavoidably causes damages to the mechanically delicate graphene [7]. To date, mass production of graphene has mainly been achieved via chemical vapour deposition (CVD) [8] and single crystal SiC epitaxial [9] growth routes. CVD graphene has been synthesised on various metal substrates such as ruthenium [10], iridium [11], platinum [6], nickel [12,13] and copper [8]. Though suitable for mass production [14], the need to transfer the graphene to different substrates has so far constrained its up-scaling to roll-to-roll production methods. Epitaxial graphene has been demonstrated to be a viable route to the production of electronic devices, such as field effect transistors [15]; however, single crystal SiC wafers are expensive and, unless SiC is required in the device, again graphene needs to be transferred. The search for better production techniques of graphene, in particular a transfer-free production method of high quality graphene, has intensified over the last few years. Recent developments include the growth of graphene from solid carbon source via rapid

---

thermal processing (RTP), for example, from Ni layer on single crystal SiC substrate [16] or from carbon containing and metal layers [17–24].

Prior to this work, direct fabrication of transistors using photolithographic process has been reported for graphene grown on Cu films deposited on SiO_2 substrate to eliminate the need of transfer [7]. However the graphene stripes in the fabricated devices were suspended on the Cu electrodes of at least 500 nm-thick as the graphene was grown atop the Cu layer and the Cu underneath the graphene channels must be etched away in acid while keeping the Cu electrode layers un-etched. It is therefore doubtful about the possibility of using such a process in industrial scale electronic devices. Direct growth of graphene on mica substrates by molecular beam epitaxy (MBE) has been attempted [24], however, only few-layer graphene with poor Raman spectrum and device performances were demonstrated. Direct growth of large area graphene on insulator substrates from solid carbon sources such as PMMA/Ni on SiO_2 [25], carbon/Ni on SiO_2 with complete Ni evaporation [26] has also been reported. Although these are interesting developments, the reported quality of graphene was incomparable to that of transferred and no device data were presented. There are also doubts about the feasibility of growing graphene at the interface between the catalytic metal and the SiO_2 substrate or the complete evaporation of Ni in the RTP process, which were the key to the reported direct growth of graphene.

Here we show a transfer-free growth technique of large area graphene from sputtered carbon source (amorphous C or SiC) and Ni layers. In contrary to some of the reports, our investigations have shown that Ni layer could not be completely evaporated in the RTP process and graphene could not grow at the interface between the catalytic Ni layer and the SiO_2 substrate. The systematic study of the growth process has led us to discover that large area graphene can be produced on the SiO_2 substrate without the need of transfer when the Ni layer is thinner than 100 nm and is removed in acid after graphene growth. This paves the way to the production of large area graphene directly on SiO_2 substrate for electronic device applications. A growth model is proposed based on detailed study of the physical structures and properties of graphene films. The in-depth understanding of the growth process could be instrumental for the further development of new techniques for the direct growth of high quality graphene on insulator substrates.

2. Experimental

The deposition of films was carried out in a three-target RF diode and magnetron sputtering machine. Typical base pressure was 2×10^{-7} Torr and Ar pressure for deposition, 3 mTorr. All targets are 6 inch in diameter and have a typical purity of 99.99%. No substrate heating was applied during the deposition of all the layers. The substrates used in this work were single side polished Si wafers with a 300 nm-thick thermally oxidised SiO_2 layer, which was referred to as the 'Si wafer' throughout the paper.

Samples were subjected to RTP either in situ or ex-situ. Details of the heating and cooling curves of the two systems are given in Fig. S1. The in situ RTP was carried out in the same vacuum chamber as the sputter-deposition using a home-made RTP apparatus with two 500 W halogen lamps and a specially designed substrate holder with water cooling and very small thermal mass. This enables the film deposition and RTP process to be carried out in the same evacuation to ensure the oxidation-free growth of graphene. The ex-situ RTP was carried out in a commercial RTP apparatus with a quartz chamber. It provides a faster heating rate than the in situ system (see Fig. S1) and with controllable cooling rates. The apparatus has eleven 1.5 kW halogen lamps for rapid temperature ramp up at a typical rate of 100 °C/s up to 1200 °C. It also has a rapid cooling capability due to a cold chamber wall design and a very small thermal mass of the quartz sample holder. The sample chamber was purged with Ar gas for one hour before the RTP process, which was also carried out in Ar atmosphere. We found this is necessary to prevent the potential oxidation of the sample. In order to achieve the growth of good quality graphene, samples needed to be annealed fresh, particularly for samples with Ni on top: surface oxidation has an adverse effect on the formation of graphene. Under optimum conditions (no oxidation occurs to the metal films), we have found no significant difference in graphene qualities produced by the two different RTP systems if the RTP temperature and time was kept the same. For all samples, we used annealing time of 120 s. We therefore refer the RTP conditions in our paper by temperature only for simplicity.

The as-grown graphene samples were etched in HCl solution to obtain transferred or transfer-free graphene. After HCl etching, the samples were cleaned in DI water several times to remove the etching residues. As-grown, transfer-free and transferred graphene films were examined by Raman spectroscopy (with a 532 nm laser). Raman maps across large areas were carried out with a step size of 30 μm. Film thicknesses and surface morphology were characterised by AFM. Bragg–Brentano geometry and grazing-incidence X-ray diffraction at 1° angle of incidence were used for the microstructural and crystallographic characterisation of the metal and SiC films. Film composition was analysed by energy dispersive analysis by x-rays (EDAX) in SEM.

For device fabrication, a rectangle of graphene film of 18 μm by 5 μm was defined by e-beam lithography and a reactive ion-etching step. Cr/Au (5/70 nm) electrical contacts were defined by a second lithographic step and deposited using a thermal evaporator. Devices with different sizes were also fabricated using photolithographic process. The measurement of the devices was carried out either under vacuum (5×10^{-4} mbar) using standard low-frequency lock-in techniques, or in atmosphere using Keithley 2602a four channel source/measurement instrument.

3. Results and discussion

3.1. Growth process and typical results

Fig. 1 shows our graphene growth process. A carbon-containing film (SiC or amorphous carbon) and a metal film (Ni) were deposited by sputtering onto a Si substrate in the order of
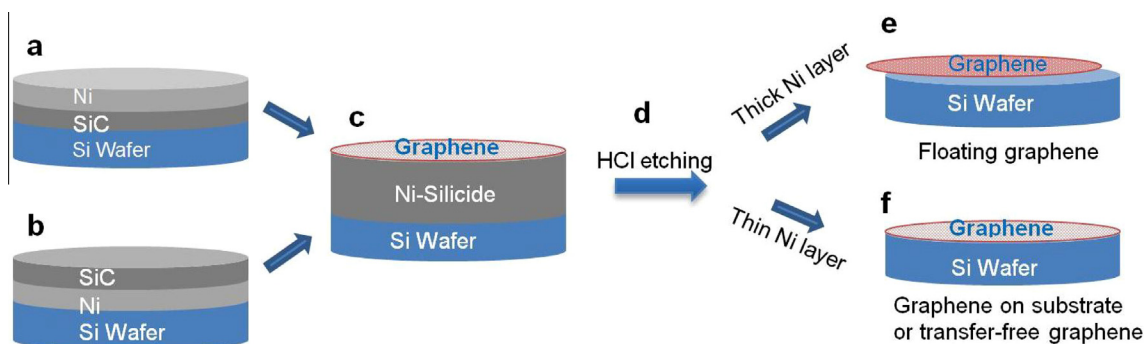
Fig. 1 – Schematic illustration of the graphene growth process. Sputter deposition of a carbon containing layer (SiC or C) and a metal film (Ni) on a thermally oxidised Si wafer in the order of either SiC/Ni (a), or Ni/SiC (b). (c) Rapid thermal processing resulting in Ni-silicidation and the formation of graphene atop the Ni-silicides upon cooling. (d) HCl etching to remove the Ni and Ni-silicide. (e) For thick Ni layer (>100 nm), after the Ni-silicide is dissolved in the HCl, graphene floats off the Si substrate and can be picked up and transferred to a new substrate. (f) For thin Ni layer (<100 nm), the graphene is retained on the original substrate.

either substrate/SiC/Ni, Fig. 1a, or substrate/Ni/SiC, Fig. 1b. After deposition, the stacks were subjected to a rapid-thermal-process at temperatures ranging from 650 to 1000 °C. (Methods and Section 1 of Supplementary information provide further details.) We find that graphene always grows atop the stack, irrespective of the deposition sequence of the two layers, Fig. 1c. After RTP, the Ni or Ni-silicide layer is etched away in HCl solution, Fig. 1d. This resulted in two possibilities: For thick Ni layers (>100 nm), Fig. 1e, after the Ni-silicide is dissolved in HCl, the graphene floats off the Si substrate and can be collected and transferred to a new substrate, which is an approach already employed by others [16,17,27]. However, if the Ni layer is sufficiently thin (<100 nm), Fig. 1f, graphene is retained on the original substrate.

Fig. 2a shows a typical Raman spectrum of graphene from sample S1 which was grown on substrate/SiC(50 nm)/Ni(500 nm) with RTP at 1000 °C for 2 min (Ex-situ 68% as shown in Fig. S1). For comparison, a spectrum of mechanically exfoliated monolayer graphene obtained by the same spectrometer is also shown. The characteristic G and 2D bands can be clearly observed. The value of the full width at half maximum (FWHM) of the symmetric 2D band and the intensity ratio of the G to 2D peaks can be used to determine the number of layers [8,28,29], with typical values <35 cm^{-1} and <0.5, respectively, for exfoliated monolayer graphene. For sample S1, both the FWHM and the G/2D ratio indicate a monolayer. These values are smaller than that of epitaxial graphene [8] and comparable with that of our comparative exfoliated sample. The lack of D band at 1350 cm^{-1} and the almost identical G peak position of the two spectra suggest that the monolayer graphene has few defects or large grains [28]. Fig. 2b shows a Raman map of the FWHM for an area of 750 μm × 500 μm of S1. The estimated surface coverage of the monolayer-like FWHM of the sample is around 40% for the mapped area. The areas of graphene on the two samples are visually identifiable, as shown by the camera shots in Fig. 2c and d for two samples (S1 and S2) with the same layer thicknesses (SiC(50 nm) and Ni(500 nm)) but reversed layer sequence (sub/SiC/Ni for S1 and sub/Ni/SiC for S2): the dark areas are graphene whilst the lighter areas are amorphous

carbon. As can be seen, samples with SiC atop Ni (Fig. 2d) produced much better graphene surface coverage than that with SiC underneath the Ni (Fig. 2c) reaching over 90% for the sample size shown in Fig. 2d. The surface morphology of the two samples can be seen from the AFM image of Fig. 2e for S1 and Fig. 2f for S2, showing that the sub/Ni-Silicide/graphene films of both samples have clearly defined crystalline grain structure with average grain size of approximately 936 nm for S1 and 564 nm for S2 although there exists considerable dispersion in grain size distribution in both samples (refer to Fig. S2 for grain size distribution of samples S1, S2 and S4). X-ray diffraction examination of the dark and lighter regions showed no significant difference in terms of phase structure and crystal texture, and also no connection between the graphene formation and the crystal orientation (see Fig. S4 for details). This is further discussed below.

3.2. Dependence on process parameters and layer thicknesses

To determine the optimal process parameters, graphene was grown from stacks with various layer thicknesses, deposition sequences and RTP conditions. Typical results are shown in Fig. 3. Fig. 3a shows two Raman spectra of sample S3 (sub/SiC(50 nm)/Ni(200 nm)) processed with RTP temperatures at 650 °C (red) and 1000 °C (blue), respectively (refer to Section 1 and Fig. S1 of Supplementary information for typical heating cooling curves). AFM images in Fig. 3a.1 and a.2 show that the re-crystallisation process of Ni film of the sample with RTP temperature of 650 °C was incomplete with a large proportion of the area containing nano-grains with typical sizes of 20–30 nm. The Raman spectrum has a FWHM value of the 2D band of 74.1 cm^{-1} and G/2D ratio of 1.77 indicating several-layer graphene for flat or exfoliated graphene films [28]. However, other reasons may also contribute to such a spectrum in this case, which will be discussed in the following sections. The D/G intensity ratio of 0.17 also suggests that the graphene contains considerable nano-grains [30]. In contrast, the same stack processed by RTP at 1000 °C produced graphene with a Raman 2D FWHM value of 47 cm^{-1} and G/2D intensity ratio
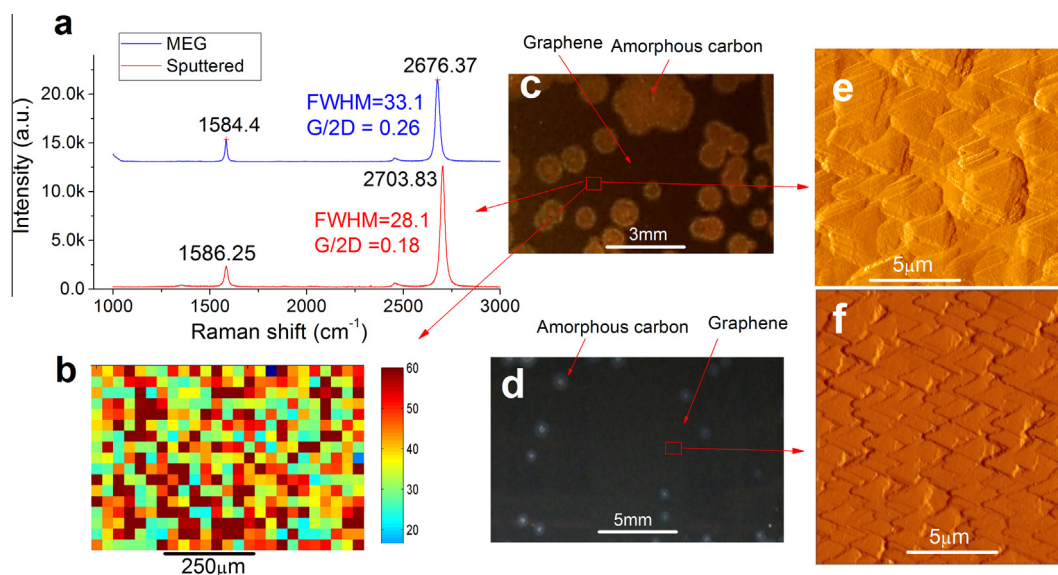
Fig. 2 – Typical characteristics of as-grown graphene. (a) Raman spectrum of as-grown graphene (red) of S1(sub/SiC(50 nm)/ Ni500(nm)). A spectrum of mechanically exfoliated monolayer graphene (MEG) on Si/SiO$_2$ substrate measured by the same Raman spectrometer is also shown for comparison (blue). Both spectra were normalised with the same G peak height. (b) Map of the FWHM of the 2D band for a surface area of 750 μm × 500 μm of S1. (c and d) Camera shots showing distinctive areas with and without graphene on S1 (c) and S2 (sub/Ni500(nm)/SiC(50 nm), with reversed layer sequence of S1 (d). (e) AFM image (amplitude contrast) of the sub/Ni-silicide/graphene surface of S1 showing typical grain sizes in the range of 1–2 μm, (f) AFM image of the sample surface of S2, showing typical grain sizes of 0.5–1 μm. (A colour version of this figure can be viewed online.)

of 0.96, indicating a bi-layer spectrum. The AFM image in Fig. 3a.3 shows that the sample is well crystallised with typical grain sizes of Ni in the range of 0.5–1.5 μm although the grain size distribution is nonuniform.

Samples with thinner SiC (or carbon) and Ni layers were also studied. No significant differences were observed by using either SiC or C sources. The Raman spectra of samples with thinner carbon/Ni layers in general showed spectra typical of few layer graphene and also with increased D band intensity indicating defected or nano-crystalline nature. Fig. 3b is a typical Raman spectrum and an AFM image of sample S4 (sub/C2.5 nm/Ni40 nm) with RTP at 1000 °C, showing a spectrum of bi or tri-layer graphene and finer grains of smaller than 1 μm. The mean grain size of the sample is approximately 500 nm (see Fig. S2c).

Fig. 3c shows the Raman spectra for two samples of different layer structure (S1 and S2) and also processed with different RTP temperatures. The two samples have the same SiC and Ni layer thicknesses as those in Fig. 2, but reversed layer sequence. The top two spectra are for S1 and S2 processed with RTP at 1000 °C. Spectrum indicative of good quality monolayer graphene (similar to the one shown in Fig. 2a) has been achieved for S1. The spectrum of S2 shows increased FWHM and G/2D ratio. As already shown in Fig. 2c and d, the surface coverage of graphene for S1 and S2 is different with S2 showing much better coverage than S1. It is also worth noting from the Raman spectra of S1 and S3 prepared in the same RTP temperature that thicker Ni films (500 nm) favour the growth of graphene with higher quality monolayer spectrum if Ni atop SiC. The two lower spectra shown in Fig. 3c are for S1 and S2 processed with RTP at a lower temperature of

700 °C. The FWHM values of the two spectra are found to be 45.8 and 55.2 cm^{-1}, respectively, suggesting bi- or tri-layer spectrum. Again, S1 (Ni atop SiC) exhibits slightly better Raman characteristics with smaller FWHM values and nearly negligible D band intensity. These results suggest that the grain size of Ni films decreases with the decrease of RTP temperature and Ni layer thickness, which results in spectra typical of multi-layer graphene. The monolayer-like spectrum was only obtainable from samples with large Ni grains (at Ni thickness of ~500 nm and RTP temperature of ~1000 °C).

Fig. 3d shows two Raman spectra of S1 prepared under the same RTP condition of 1000 °C for 2 min but with reduced cooling rate at 2%/s (2% power intensity per second) and 1%/s for the top and bottom spectrum, respectively (see Fig. S1 for cooling profile). These samples exhibit a much wider 2D band and also higher D band intensity than those with normal cooling rate at 15%/s (top spectrum of Fig. 3c). In general, it was found that the heating rate was not crucial, but a faster cooling rate favours the growth of monolayer layer graphene, which agrees with the results by Yu et al. [12].

3.3. Crystal structures and crystallographic orientation of the films after RTP

The crystal structure and crystallographic orientation of the films were examined by small angle grazing-incidence diffraction (GID) of x-rays. (Section 3 and Fig. S4 of the Supplementary information of the information give more details about the GID measurements.) Fig. 4 shows the GID patterns of samples S1, S2 and S3. All three samples exhibit preferred Ni(111) and Ni$_{17}$Si$_3$(220) orientations, indicating good
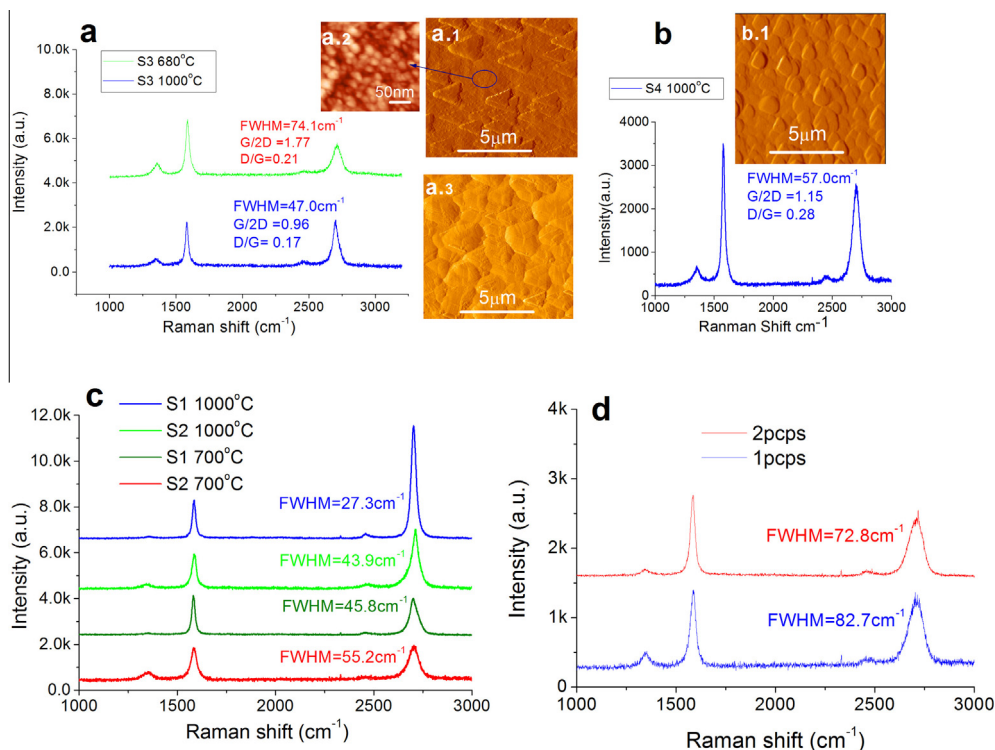
Fig. 3 – Raman spectra of as-grown graphene from samples with different Ni layer thicknesses, deposition sequences and RTP systems/conditions. (a) Raman spectra of S3 (SiC50 nm/Ni200 nm) with different RTP temperatures at 650 °C (red) and 1000 °C (blue) AFM images for S3 at 650 °C are given in a.1 and a.2, and S3 at 1000 °C, in a.3. (b) Raman spectrum of S4 (C2.5 nm/Ni40 nm) with RTP at 1000 °C. AFM for the sample is given in b.1. (c) Raman spectra of samples S1 and S2 (as those in Fig. 2) processed with two different RTP temperatures of 1000 °C (blue and light green curves) and 700 °C (dark green and red curves), respectively. (d) Raman spectra of S2 processed with slower cooling rates. (A colour version of this figure can be viewed online.)
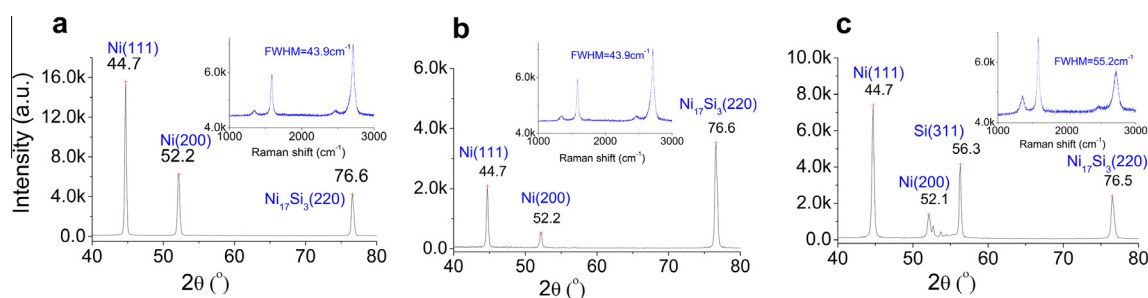
Fig. 4 – Grazing-incidence X-ray diffraction patterns for three samples. Panel a shows measurements on S1; panel b for S2. Both samples were prepared with the same RTP condition at 1000 °C. Panel c is for S3 with RTP temperature at 650 °C. The inset in each panel is the corresponding Raman spectrum of the samples.

crystallites and complete Ni-silicidation. The contrast difference in peak intensities of the Ni(111), Ni(200) and $Ni_{17}Si_3(220)$ of S1 (Fig. 4a) and S2 (Fig. 4b) suggests that there is a difference in the composition of the Ni-silicide across the depth of the films: the top surface of S1 is richer in Ni, and that of S2 is richer in Ni-silicide. (The structure on the top surface contributes more to the intensities of the diffraction peaks in GID.) This is natural, considering the different layer deposition sequence of the two samples and the relatively short RTP time (2 min), which was insufficient for a complete diffusion of the SiC throughout the whole 500 nm depth of the

Ni film. It is also natural to expect that the carbon concentration across the film depth is also non-uniform. The better surface coverage of graphene in S2 compared to S1 is a result of a top surface that is much richer in carbon. The richer carbon concentration may also contribute to the formation of smaller grains during the growth (grain refine effect [31]), as shown in Fig. 2f, and hence the resultant bi-layer like spectrum. The poorer concentration of carbon on the surface of S1 favours the growth of large grain sizes and produces monolayer-like spectrum but results in a lower surface coverage. The reasons for the formation of amorphous carbon areas remain unclear:

for instance, the existence of the $Ni_{17}Si_3(220)$ phase of S2 surface does not appear to have any adverse effect on the growth of graphene. The major difference in the GID pattern of S3 (Fig. 4c) is the presence of an additional peak of Si(311) and a relatively weaker and messy Ni(200) band. This suggests that the recrystallization and Ni silicidation processes were incomplete due to the insufficient RTP temperature (in agreement with the AFM images in Fig. 3a).

3.4. Transferrable and transfer-free graphene

The as-grown graphene samples were further processed by removing the Ni, Ni-silicide or Ni-carbide layers in HCl solution. For samples with thick Ni layers (>100 nm), the graphene film always floats off the original substrate after the removal

of the Ni in HCl. In general, the graphene film is robust and can be picked up by a piece of wafer without being visibly broken. For samples prepared with thin Ni layers (<100 nm), the graphene film can be retained on the original substrate and therefore no further transfer is required for device applications. The HCl etching step is required to remove the Ni layer as we found no evidence of Ni being fully evaporated at RTP temperatures of up to 1100 °C.

The etching of Ni appeared to take place side ways via the edges of samples as well as vertically through the grain boundaries and defects of graphene. The etching time was much longer for samples with thinner Ni layers than thicker ones, implying that the side-way etching was more dominant for samples with thicker Ni layers. Overall, the etching took quite long time (usually we left the samples in acid
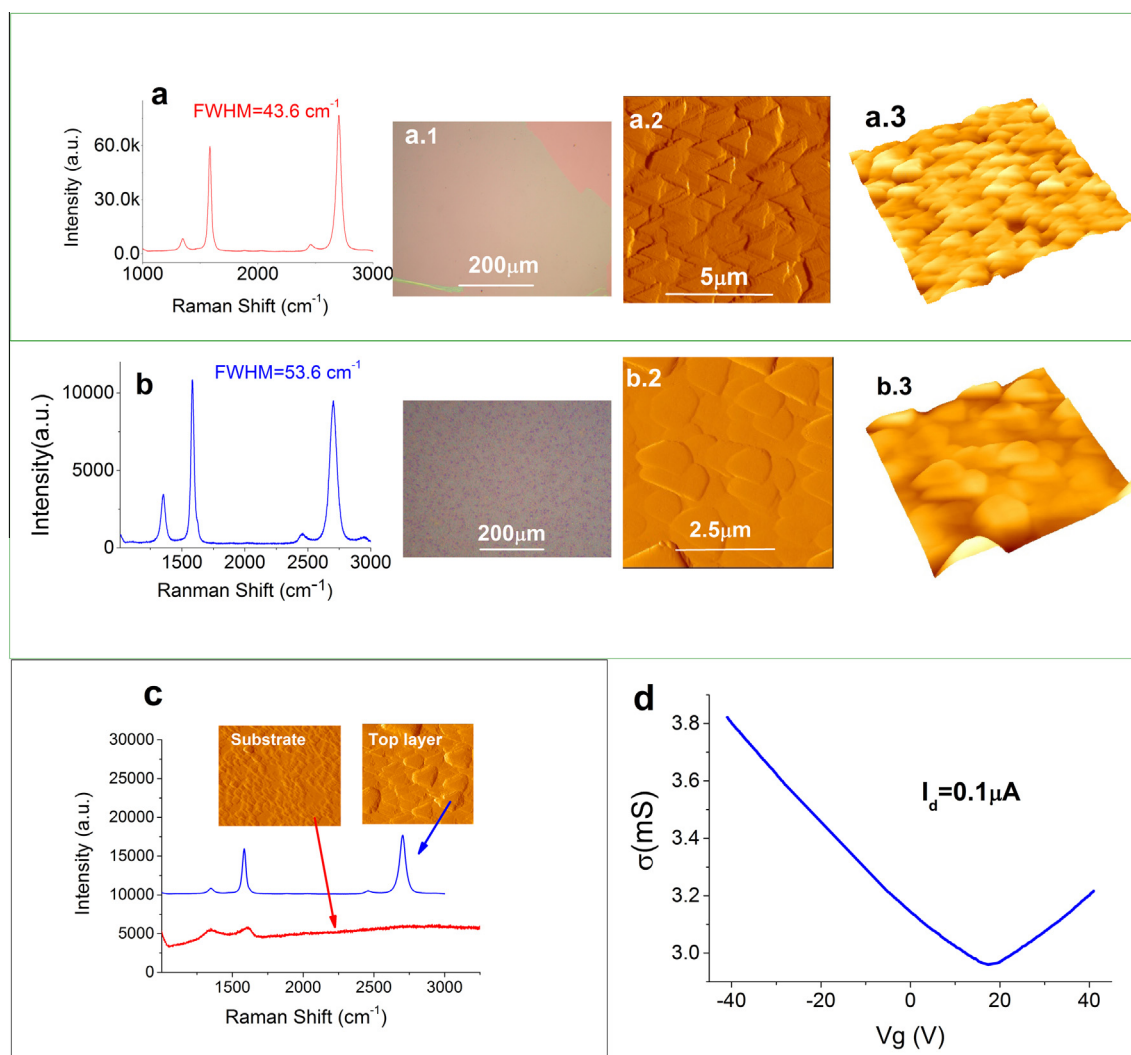
Fig. 5 – Characterisation of the transferred graphene and transfer-free graphene. (a) Raman spectrum of graphene of S2 transferred to Si substrate after removal of Ni-silicide in HCl. a.1, a.2 and a.3 are the optical micrograph, AFM amplitude contrast and AFM 3D images of the sample, respectively. (b) Raman spectrum of transfer-free graphene from S4, retained on the original substrate after the removal of Ni in HCl. b.1, b.2 and b.3 are the optical micrograph, AFM amplitude contrast and AFM 3D images, respectively, of the transfer-free graphene. (c) AFM and Raman inspections of the top graphene layer and the substrate surface after the removal of graphene by sputter-etching and the removal of Ni layer by etching in acid. (d) Electrical characterisation of a graphene field effect transistor showing modulation of the channel conductivity with back gate voltage. (A colour version of this figure can be viewed online.)

overnight), which means the graphene film was quite tight and of good quality, however etching through grain boundaries did exist as the gas bubbles accumulated on the samples after etching were visible from both edges and top surfaces. The etching of Ni was complete as no Ni or other residues could be detected by EDAX analysis for etched and cleaned graphene samples (see Fig. S6 for detail). No visible damages to the graphene film was observed either as shown by the optical microscope image in Fig. S6(b).

Fig. 5a shows a typical Raman spectrum of graphene transferred onto a silicon wafer. In comparison with the spectrum of the as-grown graphene for the same sample S2 (second spectrum from top of Fig. 3b), there is almost no change in the relative intensities of G and 2D peak and the value of the FWHM of the 2D band. However, the D peak intensity of the transferred graphene is slightly higher, which is most likely due to microscopic damage caused by the transfer process. Fig. 5a.1 is an optical microscope image of the transferred graphene film settled on a Si wafer. On the microscopic scale, the transferred graphene is not smooth but appears to replicate the morphology of the Ni surface on which it grew. Fig. 5a.2 is an AFM image (amplitude contrast) of the transferred graphene from S2, which shows well defined grains with grain sizes in the range 0.5–1.5 μm. Fig. 5a.3 is a 3D topographic AFM image of the transferred graphene showing the non-planar nature of the film morphology. It shows that graphene is formed around the surfaces of Ni grains or wrapped around and in close contact with the Ni grains. It floats off the original substrate, when the Ni is dissolved, as a rigid sheet with imprinting of the grain morphologies of the Ni film. The non-planar graphene sheet consists of flat, tilted as well as vertical surfaces with many overlaps of graphene grains of various sizes, particularly near the grain boundaries. The average roughness measured by AFM was as high as 20–40 nm and with 10 points height as high as 200 nm (Fig. S3 gives typical surface roughness measurement of the as-grown samples.) There is no significant difference in the surface morphology or roughness between the as-grown and transferred samples. This non-planar nature is in fact common to graphene grown by on all metal surfaces, e.g. CVD graphene on Cu [32] (also see Fig. S3 of Supplementary information for comparison of roughness with CVD graphene), or CVD graphene on Ni [33], mainly due to similar recrystallization process of the metal grains at similar temperatures for the growth processes. In addition, the actual size of graphene grains could be much smaller than that of the metal grains as grain boundaries are also formed from in graphene crystals even grown on the large metal crystal surfaces, as observed by Huang et al. [34] for CVD graphene on Cu. Malola et al. [35] have pointed out that graphene grain boundaries are topological defects that often have a disordered character and can be characterised by their trends in energy, atomic structure, chemical reactivity, corrugation heights, and dynamical properties as a function of lattice orientation mismatch. Graphene grown from sputtered Ni is likely to show similar characteristics as CVD graphene, i.e. the actual grain size of graphene film is much smaller than that of Ni grains. The graphene crystals are also unlikely to grow across the Ni grain boundaries without being interrupted due to the nature of the catalytic growth. We therefore believe that there are two types of graphene grain boundaries when graphene is grown on metal surfaces: the grain boundaries of graphene on large metal crystal surface due to dislocation of carbon atoms during graphene growth [34], and the grain boundaries of graphene due to the existence of the grain boundaries of metal crystals caused by multiple nucleation sites across the metal grain boundaries [33] and the physical separation of the Ni grains. The latter results in the non-planar and rough graphene morphology as observed by our AFM imaging. As the structural quality of graphene films, such as atomic flatness and low defects, is of immensely importance both to its electronic properties and devices applications, all these represent a major challenge for the growth of defect-free and atomically flat single crystal graphene films via the metal catalyst route [32,36].

Fig. 5b shows a typical Raman spectrum of transfer-free graphene of S4 after the removal of the Ni layer in HCl. Its corresponding optical microscope and AFM images are shown in Fig. 5b.1 and 5b.2, respectively. For the transfer-free graphene, the Raman spectrum is comparable with that of as-grown samples as shown in Fig. 3b although D band intensity is increased after the removal of the Ni, which perhaps indicates the microscopic damage or defects caused by HCl etching. The surface morphology of the graphene is again uneven, a replica of the morphology of the Ni layer as shown in Fig. 5b.2 and b.3, similar to those of transferred graphene of S2, but with smaller grains and also many overlaps (e.g. there is a cluster of overlapped grains visible in the middle of the AFM images). When the Ni film is dissolved in HCl, this non-planar graphene sheet with imprint of the grain morphology is retained on the original substrate.

Further studies were carried out to understand why graphene grown on thick Ni layer floats after the removal of Ni in acid whilst that on thin Ni layers stays on the original wafer. For samples with thick Ni layers, e.g. S1, S2 and S3, the surface were scanned by Raman and AFM before and after a layer of graphene floated off in HCl solution. For samples with thin Ni layers, e.g. S4, the top graphene layer was removed by sputter-etching before etching the samples in acid. Typical results are given in Fig. 5c. The Raman spectrum (upper blue curve) of Fig. 5c is taken from the top surface of a sample after RTP, which shows typical graphene signature spectrum. Its corresponding AFM image is also given (marked as top layer), showing crystalline grain structures of Ni. The bottom spectrum (red curve) was taken from the substrate surface after the removal of the top graphene and Ni layer, which shows a spectrum with weak but broad D and G bands with peaks at 1350 cm^{-1} and 1600 cm^{-1}, respectively, typical of nanocrystalline graphite (nc-G) [37,38]. The corresponding AFM image also shows some fine structures left on the substrate surface. These results confirm that graphene only grew on the top surface of the samples no matter whether they were grown from samples with Ni atop carbon, carbon atop Ni, thick Ni or thin Ni. In all cases, there was a layer of nc-G left on the original substrate after etching in HCl. As the graphene growth processes from Ni films typically involve diffusion-segregation (or precipitation) [39,40], our results show that the diffusion and precipitation of carbon atoms in Ni during the RTP cooling down phase is isotropic, i.e. carbon precipitated on all surfaces of Ni grains including the bottom interface. However,

graphene could only grow on the top surface and around the Ni grains i.e. in grain boundaries. Although a layer of carbon also precipitated at the Ni and SiO₂ interface, the proximity of the Ni with SiO₂ appeared to be preventing the growth of graphene at that interface perhaps due to the loss of the catalytic function of the Ni caused by the unfavourable chemistry at Ni/SiO₂ interface. Thus, for samples with thick Ni layers, the graphene in the vertical plane became discontinuous due to the lack of continuous Ni grain boundary surfaces down the substrate, and therefore the graphene film floats off the substrate once the Ni is dissolved as there is no physical contact between the top graphene layer and the bottom nc-G layer. For samples with thinner Ni (in the range of <100 nm), there are sufficient surface areas around the grain boundaries right down to the substrate for graphene to reach the substrate surfaces where it joins with the nc-G layer, which serves as anchors for retaining the graphene sheets on the original wafer. However, most of the surface areas of graphene are suspended in air without physical contact with the substrate.

Electrical characteristics of back-gated graphene field-effect transistor made from transfer-free graphene were measured on a number of devices and a typical result is shown in Fig. 5d. Ambipolar IV characteristics were observed with charge neutrality Dirac voltage of $V_D \sim 17$ V. The gate modulation caused a change in conductivity of ~0.85 mS over the measurement range, which is approximately 29%. The gate modulation is not as effective as that expected from exfoliated samples [41], however comparable with graphene grown by other routes [17,42]. Devices made from transfer-free graphene in general showed better results than those made from transferred graphene although the device performance also depends strongly on the location of the device element and the microfabrication process.

3.5. The growth model

From these results we propose a growth model for graphene grown from sputtered carbon and Ni films (Fig. 6). Fig. 6a shows an ideal case where graphene is grown on a thick Ni layer with sufficiently large and uniform grains of Ni formed during RTP. For each large Ni grain, monolayer graphene is formed on the top surface and around the grains (a.1) due to the relatively smooth top surface. Such a sample would exhibit Raman spectrum typical of monolayer as that shown in Fig. 2a. However, in practice uniform and large Ni grains are hard to achieve across the whole wafer due to many factors which may affect the size of Ni grains during RTP, the monolayer graphene coverage could only be achieved in patches, around 40% as shown by the Raman mapping in Fig. 2b. At the interface of the Ni and SiO₂ substrate, a layer of nc-G is also formed as a result of isotropic precipitation of C from Ni, as evidenced by the AFM image and Raman spectrum of Fig. 5c. We found that the nc-G layer has a good adhesion with the substrate. However, graphene will float off the substrate after the removal of the Ni in acid as there is no physical link between the top graphene layer and the bottom nc-G layer (a.2). Fig. 6b refers to the case for the growth of transfer-free graphene, where smaller and irregular Ni grains were formed during RTP due to thinner Ni layers. Graphene is formed around Ni grains and grain boundaries right through to the substrate, where it links up with the nc-G (b.1). Due to the bonding between the graphene and the nc-G layer on the substrate, the graphene is retained on the original wafer upon removal of the Ni in acid (b.2), as evidenced by AFM images and Raman spectrum shown in Fig. 5b for S4. For samples with Ni thickness thinner than 30 nm, we have observed that the graphene layer is no longer continuous because of the recrystallization and de-wetting of Ni grains during RTP, which
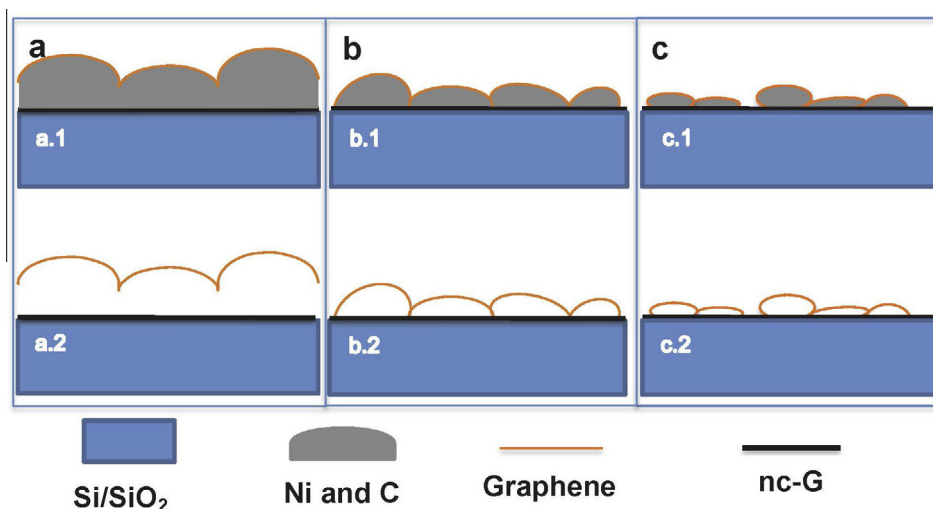
Fig. 6 – Schematic illustration of the growth model. (a) Thick Ni layer (>100 nm) with large grains: graphene grows atop of the stack and replicates the grain morphology of Ni and an nc-G layer is also formed at the interface of Ni and SiO₂ (a.1). A floating monolayer graphene sheet (a rigid imprint of the Ni topography) is obtained after the removal of Ni in acid (a.2). (b) Thin Ni layer (30–100 nm): graphene atop of the stack can grow through the grain boundaries and link up with the nc-G layer on the substrate surface (b.1). Graphene remains on the original substrate as a rigid imprint of the Ni topography when the Ni is removed in acid (b.2). (c) Small Ni grains in grain boundaries: monolayer graphene also grows around these small Ni grains (c.1). The resultant graphene sheet has overlapped grains across the grain boundaries due to the irregular grain structures of the Ni (c.2). (A colour version of this figure can be viewed online.)

resulted in discontinuous Ni films. Fig. 6c. depicts the situation where, due to the abundance of nucleation sites at the grain boundaries, more small Ni grains are formed, which result in small grains of graphene in these areas overlapping with each other, for example those shown in Fig. 5b and c. Although graphene formed on each Ni grain is likely to be monolayer, these overlapped grains may produce a Raman spectrum typical of bi or few layer graphene. The smaller the grain size, the more percentage of these overlapped areas exist and therefore make the Raman spectrum look more like multi-layer graphene. This makes the interpretation of Raman results for these samples more complicated than for exfoliated planar graphene. It is therefore arguable that graphene grown on Ni may be self-limiting to monolayer growth as far as each individual Ni grain is concerned as graphene could only grow around and in close contact with the Ni grains. The few-layer like Raman spectra could be mainly due to the contribution of overlapped graphene grains in the grain boundaries. Further experimental studies are required in order to clarify these issues.

4.　　Conclusions

Large area graphene in either transfer-free or transferrable form can be grown from sputtered carbon and metal layers on Si wafers with RTP. Graphene always grows atop the stack, around Ni grains and in close contact with Ni. The resultant graphene sheet is rigid and uneven, a replica of Ni surface morphology, which is comparable with CVD graphene on Cu. A layer of nc-G on the substrate is also observed, perhaps as a result of isotropic diffusion-precipitation of carbon from Ni grains and the unfavourable chemistry at Ni-SiO$_2$ interface for the growth of graphene. Transfer-free graphene is produced on SiO$_2$ insulator substrate with the removal of Ni in acid when Ni thickness is in the range of 30–100 nm, which pave the way to the production of large scale graphene directly on SiO$_2$ insulator wafers. The characteristics of Raman spectrum depend on the size of Ni grains, which in turn depend on the thickness of Ni, layer deposition sequence of the stack and RTP temperature. A model is proposed to illustrate the graphene growth process. It is understood from our results that graphene grown on Ni film may be self-limiting on each individual Ni grain perhaps via catalytic growth as no connection between the graphene formation and the crystal orientation was observed. The microscopic scale non-planar morphology of the graphene films with overlapped grain boundaries introduces complications in the interpretation of the Raman data. It also represents a major challenge to the mass production of defect-free and atomically flat graphene films for device applications.

Acknowledgments

Appendix A.　Supplementary data

Supplementary data associated with this article can be found, in the online version, at http://dx.doi.org/10.1016/j.carbon.2013.08.036.

REFERENCES

[1] Geim AK. Graphene: status and prospects. Science 2009;324(5934):1530–4.
[2] Geim AK, Novoselov KS. The rise of graphene. Nat Mater 2007;6(3):183–91.
[3] Liao L, Lin Y-C, Bao M, Cheng R, Bai J, Liu Y, et al. High-speed graphene transistors with a self-aligned nanowire gate. Nature 2010;467(7313):305–8.
[4] Lin Y-M, Dimitrakopoulos C, Jenkins KA, Farmer DB, Chiu H-Y, Grill A, et al. 100-GHz transistors from wafer-scale epitaxial graphene. Science 2010;327(5966):662.
[5] Castro Neto AH, Guinea F, Peres NMR, Novoselov KS, Geim AK. The electronic properties of graphene. Rev Mod Phys 2009;81(1):109.
[6] Ryoko O et al. Electronic states of monolayer graphene on Pt(755) and TiC(755). Tanso 2000;195:400–4.
[7] Levendorf MP, Ruiz-Vargas CS, Garg S, Park J. Transfer-free batch fabrication of single layer graphene transistors. Nano Lett 2009;9(12):4479–83.
[8] Li XS, Cai WW, An JH, Kim S, Nah J, Yang DX, et al. Large-area synthesis of high-quality and uniform graphene films on copper folis. Science 2009;324(5932):1312–4.
[9] Berger C, Song ZM, Li TB, Li XB, Ogbazghi AY, Feng R, et al. Ultrathin epitaxial graphite: 2D electron gas properties and a route toward graphene-based nanoelectronics. J Phys Chem B 2004;108(52):19912–6.
[10] Sutter PW, Flege JI, Sutter EA. Epitaxial graphene on ruthenium. Nat Mater 2008;7(5):406–11.
[11] Coraux J, N'Diaye AT, Busse C, Michely T. Structural coherency of graphene on Ir(111). Nano Lett 2008;8(2):565–70.
[12] Yu Q, Lian J, Siriponglert S, Li H, Chen YP, Pei S-S. Graphene segregated on Ni surfaces and transferred to insulators. Appl Phys Lett 2008;93(11):113103-3.
[13] Kim KS, Zhao Y, Jang H, Lee SY, Kim JM, Kim KS, et al. Large-scale pattern growth of graphene films for stretchable transparent electrodes. Nature 2009;457(7230):706–10.
[14] Moon JS, Curtis D, Hu M, Wong D, McGuire C, Campbell PM, et al. Epitaxial-graphene RF field-effect transistors on Si-face 6H-SiC substrates. Electron Device Lett, IEEE 2009;30(6):650–2.
[15] Novoselov KS, Geim AK, Morozov SV, Jiang D, Zhang Y, Dubonos SV, et al. Electric field effect in atomically thin carbon films. Science 2004;306(5296):666–9.
[16] Juang Z-Y, Wu C-Y, Lo C-W, Chen W-Y, Huang C-F, Hwang J-C, et al. Synthesis of graphene on silicon carbide substrates at low temperature. Carbon 2009;47(8):2026–31.
[17] Hofrichter J, Szafranek BuN, Otto M, Echtermeyer TJ, Baus M, Majerus A, et al. Synthesis of graphene on silicon dioxide by a solid carbon source. Nano Lett 2009;10(1):36–42.
[18] Liu N, Fu L, Dai B, Yan K, Liu X, Zhao R, et al. Universal segregation growth approach to wafer-size graphene from non-noble metals. Nano Lett 2010;11(1):297–303.
[19] Sun Z, Yan Z, Yao J, Beitler E, Zhu Y, Tour JM. Growth of graphene from solid carbon sources. Nature 2010;468(7323):549–52.
[20] Yan Z, Peng Z, Sun Z, Yao J, Zhu Y, Liu Z, et al. Growth of bilayer graphene on insulating substrates. ACS Nano 2011;5(10):8187–92.

[21] Liu X, Fu L, Liu N, Gao T, Zhang Y, Liao L, et al. Segregation growth of graphene on Cu–Ni alloy for precise layer control. J Phys Chem C 2011;115(24):11976–82.

[22] Kwak J, Chu JH, Choi J-K, Park S-D, Go H, Kim SY, et al. Near room-temperature synthesis of transfer-free graphene films. Nat Commun 2012;3:645.

[23] Zheng M, Takei K, Hsia B, Fang H, Zhang X, Ferralis N, et al. Metal-catalyzed crystallization of amorphous carbon to graphene. Appl Phys Lett 2010;96(6):063110.

[24] Lippert G, Dabrowski J, Lemme M, Marcus C, Seifarth O, Lupina G. Direct graphene growth on insulator. Phys Status Solidi B 2011;248(11):2619–22.

[25] Peng Z, Yan Z, Sun Z, Tour JM. Direct growth of bilayer graphene on SiO_2 substrates by carbon diffusion through nickel. ACS Nano 2011;5(10):8241–7.

[26] Xiong W, Zhou YS, Jiang LJ, Sarkar A, Mahjouri-Samani M, Xie ZQ, et al. Single-step formation of graphene on dielectric surfaces. Adv Mater 2013;25(4):630–4.

[27] Lee DS, Riedl C, Krauss B, von Klitzing K, Starke U, Smet JH. Raman spectra of epitaxial graphene on SiC and of epitaxial graphene transferred to SiO_2. Nano Lett 2008;8(12):4320–5.

[28] Ferrari AC, Meyer JC, Scardaci V, Casiraghi C, Lazzeri M, Mauri F, et al. Raman spectrum of graphene and graphene layers. Phys Rev Lett 2006;97(18):187401.

[29] Emtsev KV, Bostwick A, Horn K, Jobst J, Kellogg GL, Ley L, et al. Towards wafer-size graphene layers by atmospheric pressure graphitization of silicon carbide. Nat Mater 2009;8(3):203–7.

[30] Cancado LG, Takai K, Enoki T, Endo M, Kim YA, Mizusaki H, et al. General equation for the determination of the crystallite size L[sub a] of nanographite by Raman spectroscopy. Appl Phys Lett 2006;88(16):163106-3.

[31] Jin Q, Eom J-P, Lim S-G, Park W-W, You B-S. Grain refining mechanism of a carbon addition method in a Mg–Al magnesium alloy. Scripta Mater 2003;49(11):1129–32.

[32] Zhu S-E, Calado VE, Vandersypen LMK, Janssen GCAM. Controllable synthesis of large monlayer and multilayer graphene crystal. Graphene 2013. also private communication. Bilbao, Spain, 2013.

[33] Zhang Y, Gomez L, Ishikawa FN, Madaria A, Ryu K, Wang C, et al. Comparison of graphene growth on single-crystalline and polycrystalline Ni by chemical vapor deposition. J Phys Chem Lett 2010;1(20):3101–7.

[34] Huang PY, Ruiz-Vargas CS, van der Zande AM, Whitney WS, Levendorf MP, Kevek JW, et al. Grains and grain boundaries in single-layer graphene atomic patchwork quilts. Nature 2011;469(7330):389–92.

[35] Malola S, Häkkinen H, Koskinen P. Structural, chemical, and dynamical trends in graphene grain boundaries. Phys Rev B 2010;81(16):165447.

[36] Zakar E, Nichols BM, Kilpatrick S, Meissner G, Fu R, Hauri K. Nucleation sites for multilayer graphene on nickel catalyst. Nanotechnology (IEEE-NANO), 2011 11th IEEE Conference on; p. 1516–20.

[37] Ferrari AC, Robertson J. Interpretation of Raman spectra of disordered and amorphous carbon. Phys Rev B 2000;61(20):14095–107.

[38] Chu PK, Li L. Characterization of amorphous and nanocrystalline carbon films. Mater Chem Phys 2006;96(2–3):253–77.

[39] Shelton JC, Patil HR, Blakely JM. Equilibrium segregation of carbon to a nickel (111) surface–surface phase-transition. Surf Sci 1974;43:493–520.

[40] Reina A, Thiele S, Jia X, Bhaviripudi S, Dresselhaus M, Schaefer J, et al. Growth of large-area single- and Bi-layer graphene by controlled carbon precipitation on polycrystalline Ni surfaces. Nano Res 2009;2(6):509–16.

[41] Chen J-H, Jang C, Xiao S, Ishigami M, Fuhrer MS. Intrinsic and extrinsic performance limits of graphene devices on SiO_2. Nat Nanotechnol 2008;3(4):206–9.

[42] Reina A, Jia X, Ho J, Nezich D, Son H, Bulovic V, et al. Large area, few-layer graphene films on arbitrary substrates by chemical vapor deposition. Nano Lett 2008;9(1):30–5.